DOI 10.1007/s11141-024-10323-w
*Radiophysics and Quantum Electronics, Vol. 66, Nos. 7–8, December, 2023*
*(Russian Original Vol. 66, Nos. 7–8, July–August, 2023)*

# MAGNETIC SYSTEM OF A SUB-GIGAWATT FREE-ELECTRON LASER OF THE TERAHERTZ RANGE BASED ON A KILOAMPERE BEAM OF RELATIVISTIC ELECTRONS

**E. S. Sandalov,[1*] S. L. Sinitsky,[1] A. V. Arzhannikov,[1]**
**V. A. Pavlyuchenko,[1] P. A. Bak,[1] N. S. Ginzburg,[1]**
**P. V. Logachev,[1] I. N. Mescheryakov,[1]**
**D. A. Nikiforov,[1] N. Yu. Peskov,[1] R. V. Protas,[2]**
**K. K. Ryabchenko,[1] and D. I. Skovorodin[1]**

UDC 537.8+621.384.6

*We consider the project of a sub-gigawatt free-electron laser (FEL) in the THz range based on a high-current electron beam proposed in 2020 by a scientific collaboration team from G. I. Budker Institute of Nuclear Physics of the Siberian Branch of the Russian Academy of Sciences (BINP SB RAS, Novosibirsk) and the Institute of Applied Physics of the Russian Academy of Sciences (Nizhny Novgorod). A new generation of linear induction accelerators (LIA) with a kiloampere current level and an energy of up to 10 MeV, which are capable of forming beams with a high current density and low normalized emittance, is developed at the BINP SB RAS and can be used as a source of an electron beam for such a FEL generator. The objective of our research is to develop and create a FEL generator producing pulses of coherent radiation in the THz range with a sub-GW power level and a record-breaking energy content in a pulse of about* 10–100 *J. Combination of a high current density of the beam and its long pulse duration (about 100 ns) together with a small spread in the longitudinal electron velocities of the beam opens up the possibility of implementing the FEL scheme in two different types of oversized electrodynamic systems. The first is based on a two-mirror Bragg resonator, in which waves are reflected due to the coupling of the traveling and quasi-critical waves on a corrugated surface. In the second type of the electrodynamic system, a quasi-optical resonator based on the Talbot effect is used. According to the theory, the simulation results, and the data of the cold experiments, both schemes make it possible to ensure a stable regime of narrow-band generation of THz radiation under the conditions of significant cavity oversize, i.e., the ratio of the cavity diameter and the radiation wavelength* ($\phi/\lambda > 30$–$40$)*. The main structural elements of the developed section of the FEL generator and their design parameters are discussed within the framework of this article. When developing the magnetic system of this section, we calculated the time dependence of the spatial configurations of pulsed magnetic field in a helix undulator with a period of* $d = 10$ *cm and a length of 2 m, as well as in the solenoid of a quasi-homogeneous magnetic field of the same length intended for compression of the beam cross section before its input in the vacuum channel of the FEL section and for consequent transport of the beam inside it. The presented results of modeling and testing of the manufactured elements for the FEL section will become the basis for the design of a high power FEL generator operated in the frequency range from 0.3 to 1.2 THz.*

* E.S.Sandalov@inp.nsk.su

[1] G. I. Budker Institute of Nuclear Physics of the Siberian Branch of the Russian Academy of Sciences, Novosibirsk; [2] E. I. Zababakhin All-Russian Scientific Research Institute Of Technical Physics, Snezhinsk, Russia.
Translated from Izvestiya Vysshikh Uchebnykh Zavedenii, Radiofizika, Vol. 66, Nos. 7–8, pp. 538–554, July–August 2023. Russian DOI: 10.52452/00213462_2023_66_07_538 Original article submitted May 30, 2023; accepted July 25, 2023.

 

## 1. INTRODUCTION

The project of a high-power free-electron laser (FEL), which is operated in the range from subterahertz to terahertz frequencies, is currently being developed by the team of collaborators from the Institute of Nuclear Physics (INP) of the Siberian Branch of the Russian Academy of Sciences (Novosibirsk), the Institute of Applied Physics (IAP) of the Russian Academy of Sciences (Nizhny Novgorod), and the All-Russian Scientific Research Institute Of Technical Physics (VNIITF, Snezhinsk) [1, 2]. The project is based on the new generation of linear induction accelerators (LIAs), which was developed and manufactured at INP in cooperation with VNIITF [3–5]. The calculations described in [1, 2] showed that the FEL generator in the above-specified project can be driven by a relativistic electron beam generated in such an accelerator at a kiloampere current level, an electron energy of up to 10 MeV, and the normalized beam emittance 500–$1000\,\pi \cdot$ mm$\cdot$ rad. The use of such a beam allows one to implement the schemes of long-pulse FEL generators of coherent radiation with the subgigawatt power level and the pulse energy being 10–100 J within the above-specified ranges.

It should be noted that starting from the 1960s, the development of high-power sources of electromagnetic radiation and related studies of the interaction of this radiation with matter are of enormous interest for scientists working in many research fields. A great number of papers published in these fields was aimed at creating and studying experimentally the new mechanisms for generation of electromagnetic radiation. On this basis, new sources of radiation were developed with various values of the frequency range, power, and pulse energy. The advance in this field affected significantly the discovery and studies of new phenomena in physics, chemistry, biology, and medicine, in particular, using the spectroscopy methods [6, 7]. At present, it is of the greatest interest to develop the studies aimed at creating sources of terahertz radiation [6–13] within the so-called terahertz gap (1–10 THz). Most of the terahertz sources used currently in this range (semiconductor generators, quantum cascade lasers, solid-state generators with optical pumping, etc.) are based on semiconductor technologies, as well as nonlinear interaction of optical laser pulses with crystals [14–17]. However, the significant drawbacks of these methods are the low level of the generated continuous-wave power (in the 0.1–1.0 W range) and the impossibility to ensure fast tuning of the generation frequency within the operating frequency range [18–20]. As far as pulse devices are considered, those that are developed using the vacuum electronics methods are capable of generating microsecond pulses at a power level of hundreds of kilowatts in the frequency range about 0.7 THz [21], and the power level decreases fast to several kilowatts as the frequency increases.

It should be noted that alternative methods for generation of high-power pulses of terahertz electromagnetic radiation are developed actively at INP and IAP. For example, within the framework of this research line, the mechanisms of generation of the millimeter and submillimeter radiation during the interaction of beams with plasmas are studied [22–25]. Interest in these studies is determined by two main reasons. From the viewpoint of the basic science, these experiments will allow obtaining new data on the processes of generation of terahertz radiation under the conditions of development of the beam instability including such processes as conversion of plasma waves to electromagnetic oscillations at plasma density gradients and merging of two plasma waves into an electromagnetic wave [23–27]. From the application viewpoint, these studies at a power of a microsecond terahertz pulse of about 10 MW, which has been already achieved, give grounds to expect that the power level of several tens of megawatts can be achieved for a pulse duration of about 10 $\mu$s in the 0.1–1 THz frequency range and fast tuning of the characteristic radiation frequency by varying the plasma density.

Another well-known method of generation of millimeter and submillimeter waves is the use of free-electron lasers (FELs). The key feature of this method is that it can be used to generate high-power coherent quasimonochromatic radiation in the terahertz frequency range. Moreover, one can vary the energy of the beam electrons to change the radiation wavelengths and, despite the fact that the pulse duration can be very short, it is possible to obtain a high power of radiation [12, 18]. These properties make FELs highly attractive as sources of coherent terahertz radiation. However, the advantages of this method of generation

of terahertz radiation in this range are counterbalanced by certain disadvantages, such as intricacy of the electrodynamic and magnetic systems of the FEL and the large size and high cost of the beam accelerator. At the same time, at present no other source of terahertz radiation can compete with FELs, both in terms of the pulse power and the energy content. That is why many scientific centers and laboratories in Germany, UK, USA, Korea, China, Japan, Russia, and other countries of the world carry out research in the field of development and creation of FEL generators operating in the above-specified range [28–35].

A fundamental difference between the FEL scheme that we are developing and the terahertz FELs implemented earlier is that the terahertz radiation is generated by using a long-pulse electron beam with a pulse duration of about 100 ns and a great current density, which excites and pumps one of the modes of an oversized electrodynamic structure based on a Bragg cavity or a Talbot-type quasioptical cavity [1, 2].

This paper presents the current stage of the development of the FEL generator project and describes the structural elements of the generator and the results of simulating the operation of the elements of its magnetic systems, in particular, the helical undulator and the solenoid of the compression system, which are designed for pumping of the beam oscillations and transporting the beam in the vacuum channel of the FEL, respectively. It also presents the results of testing the manufactured elements of the magnetic system. When developing its design, we took into account specific features of the electron beam generation in the electron-optical system of the injector, as well as acceleration of the beam electrons in the magneto-optical structure of the inductive accelerator. The general FEL scheme and the experiment on generation of terahertz radiation are described in Sec. 2. Section 3 presents the results of simulating and designing the elements of the magnetic system of the FEL. The final Section 4 contains the main conclusions based on the results obtained.

## 2. GENERAL SCHEME OF THE FEL GENERATOR

One of the main problems in creating a FEL based on an electron beam, which is fed to its input from the accelerating structure of an LIA, is to form a beam with parameters acceptable for efficient generation of terahertz waves in the electrodynamic system used . In our case, two variants of such systems are considered: (i) a system based on the Bragg cavity, and (ii) a Talbot-type cavity with the characteristic oversize parameter $\varnothing/\lambda \sim 30$–$40$, where $\varnothing$ is the internal diameter of the cavity and $\lambda$ is the wavelength of the generated radiation [2, 35, 36]. Other important parameters that determine the efficiency of generation of terahertz waves by a beam are the energy spread of the beam electrons and the normalized transverse emittance of the beam. The estimations in [36] yield that in order to achieve the maximum generation efficiency, it is sufficient to ensure that the beam parameters stay below 1–2% and $1000\,\pi \cdot$ mm·mrad, respectively. Since the value of the transverse emittance of the beam at the LIA output [37] is already close to this limitation, the main requirement, which is imposed on the configuration of the magnetic system of the FEL generator in order to maintain the emittance value, is the adiabatically smooth magnetic compression of the electron beam. As shown by the calculations of this magnetic system [36], in order to maintain the beam emittance at a level close to the initial value, it is sufficient to ensure the degree of the adiabaticity of the magnetic-field increase, at which the ratio of the amplitude of the oscillations in the radius of the compressed beam in a homogeneous magnetic field of a FEL section and the average beam radius does not exceed 10%. When this value is exceeded, the own electric and magnetic fields of the beam, which are created by the volume distributions of the charge and current densities, as well as by the surface charges and currents induced at the walls of the vacuum tube of the beam drift, lead to a significant increase in the beam emittance [37]. It should also be noted that the contribution of aberrations of these elements to the beam emittance can also be significant without thorough engineering of the design of the magnetic FEL elements based on the simulation of the beam transportation in the magnetic field of this system.

Thus, in order to generate terahertz radiation in a FEL with maximum efficiency, it was necessary to make a magnetic system, which ensured smooth compression of the beam over its cross section from the initial diameter $d_1 = 40$ mm at the LIA output to the diameter $d_2 = 6$ mm in the cavity and further stable transportation of the beam to a distance of about 2 m in the magnetic field of the FEL. The chosen

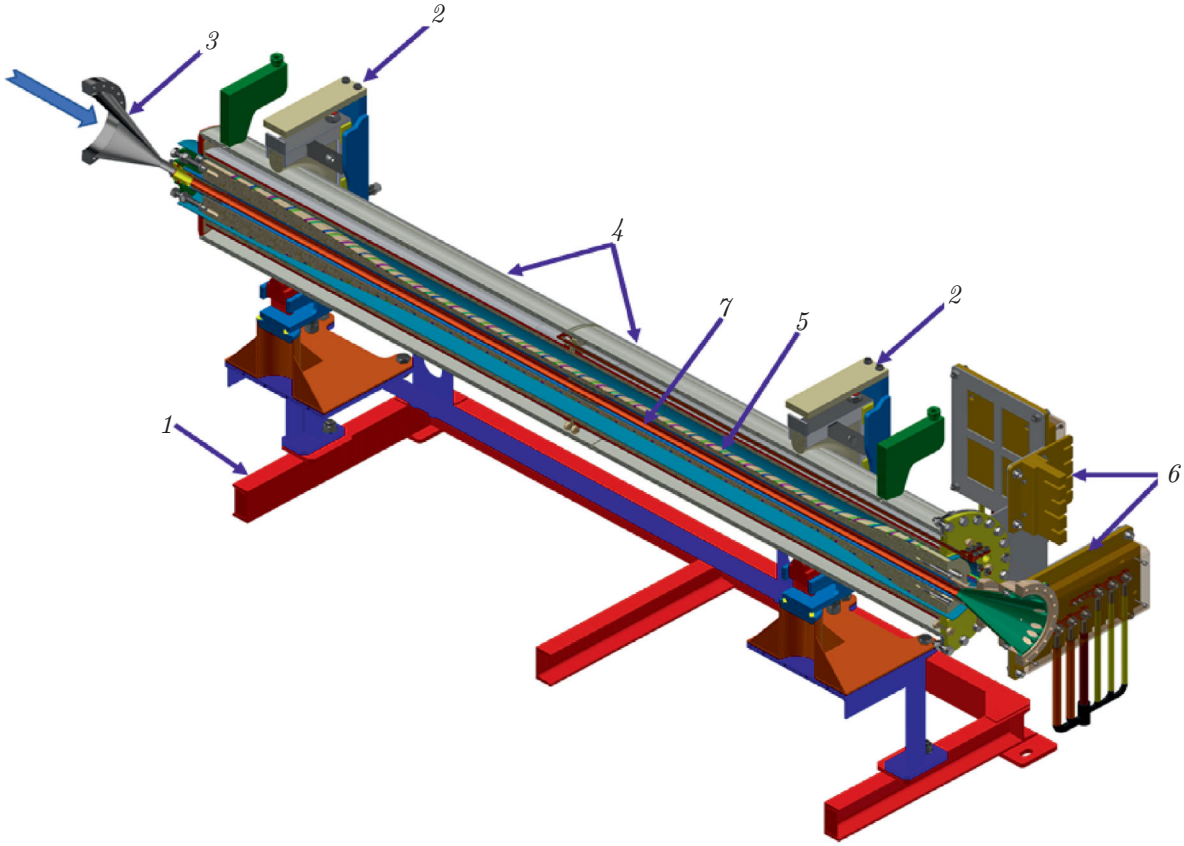


Fig. 1. Sectional view of a FEL section: supporting fixture *1*, system for FEL section positioning *2*, input section of the vacuum FEL chamber *3*, solenoid of the magnetic system, which consists of two sections installed in a magnetic cylindrical shield *4*, *5* helical undulator *5*, platforms for installation of current guides from power sources *6*, and electrodynamic system of the FEL *7*. The arrow on the left shows the electron beam conditionally.

diameter of the compressed beam was determined by the size of the region of the transverse homogeneity of the undulator magnetic field that pumped the transverse oscillations of the electrons with allowance for the amplitude of these oscillations.

In order to check the possibility of achieving strong compression of the beam diameter and test the computer codes used to simulate the beam dynamics in a FEL, we performed preliminary experiments on magnetic compression and further transportation of the high-current beam in a smooth drift tube with the diameter coinciding with the cavity diameter [36, 38]. In this set of experiments, a LIA beam with a particle energy of 5 MeV and a current of 1 kA, which was compressed by a magnetic field from the initial diameter of 40 mm to less than 10 mm in diameter, was transported in the tube drift with a diameter of 20 mm to a distance of 600 mm. Despite the great spread of the beam electron energies $\Delta E/E > 5\%$ during the current pulse [36], which was determined by an insufficient level of time synchronization of the accelerating LIA sections, the transmission of about 90% of the beam current in the above-specified drift tube was observed in these preliminary experiments.

At present, the spread in the beam particle energies is reduced to 1% in this operation regime, and the measures are taken to decrease the amplitude of spurious oscillations of the beam centroid at the accelerator output due to the development of transverse instabilities in it [39, 40]. Thus, the results of the preliminary set of experiments confirm the possibility to compress kiloampere beams with a particle energy of 5–7 MeV and transport them in a tube with the diameter coinciding with the diameter of the cavity, thus revealing the opportunity to apply such beams in the proposed FEL generator.

Figure 1 shows the scheme of the general design concept for the developed FEL, which is installed in the region of the energy output from the LIA. It is seen in the figure that the FEL consists of the following

main design elements. Fixture *1* made of steel supports system *2* for precise positioning of the FEL vacuum channel relative to the axis of the accelerating LIA system, which allows one to adjust the channel position with respect to both the spatial coordinates and the angular position in space. Vacuum chamber *3* of the FEL has a regular cylindrical part with a diameter of 38 mm and a length of 2 m, which is connected to two tapering expanders coupled with a cavity tube that has an internal diameter of 20 mm at points where the beam is input to and output from it. The distribution of the electric field in the motion region of the intense beam, which is determined by the shape of the expanders, was chosen by means of the simulation in combination with the configuration of the magnetic field in such a way as to ensure smooth compression and transportation of the beam with minimal beats of the envelope inside the cavity under the conditions of strong influence of its inherent fields.

Solenoid *4* of the magnetic system, which generates the quasihomogeneous magnetic field inside the cavity, consists of two tandem sections installed inside a magnetic cylindrical shield. Each section is equipped with built-in dipole windings for correction of the magnetic axis. The sections of the solenoid and dipole windings are powered by individual controllable switched-mode power supplies. Magnetic undulator *5* together with the solenoid of the magnetic system produces the helical magnetic field required for pumping of the transverse oscillation of the beam electrons. The platforms for installation of the current guides from power supplies *6* to the elements of the magnetic FEL system allow one to feed the windings compactly with no significant perturbations in the structure of the magnetic field in the region of the beam transportation in the electrodynamic system *7*. The design provides for the possibility to use two significantly different variants of the cavity. The first type of the cavity based on modified Bragg reflectors about 10 cm long has a length of about 2 m and an internal diameter of 20 mm (the oversize parameter is about 20–40). The second cavity is implemented within the framework of the quasioptical approach using the Talbot effect. It has a length of about 80 cm and the same internal diameter [41, 42]. The results of cold measurements of the electrodynamic properties of the developed cavities are presented extensively in [42]. Further along the beam propagation trajectory, the radiation output section will be connected, where the radiation flow will be segregated from the beam of relativistic electrons.

## 3. MAGNETIC SYSTEM OF THE FEL

### 3.1. System for magnetic compression and transportation of the beam

As it has been stated above, the preliminary experiments on compression of the cross section of the beam planned to be used in a FEL have been already performed [36, 40]. As opposed to the compression scheme described earlier [40], it is expected that the compression and transportation of the beam in the cavity will be performed by using the magnetic field of two sequential sections of the solenoid having a total length of 2 m. The current windings of these sections have a gap 4 mm wide, which is determined by the thickness of the insulating partition between them. The general view of such a solenoid consisting of two sections is shown in Fig. 2. In order to suppress the scattered magnetic fields, this solenoid is installed in a magnetic shield made of magnetically soft steel 10 as a pipe with side flanges. The main parameters of the sections of the solenoid and the magnetic shield are listed in Table 1, where the maximum current in the section windings and the component $B_z$ (where $z$ is the longitudinal coordinate) of the magnetic field on the axis at the center of the magnetic system are given for

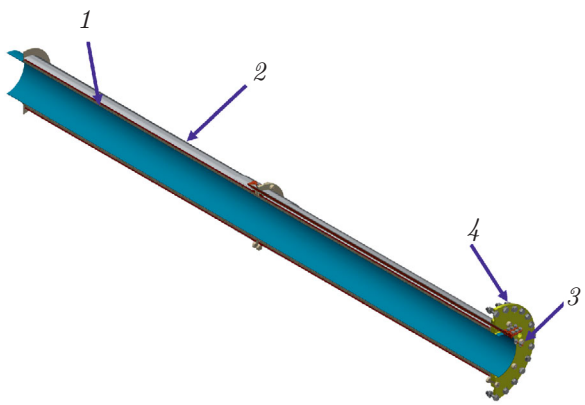


Fig. 2. Diagram of the magnetic system for compression and transportation of the beam: (*1*) pipe of stainless steel with the solenoid fixed on it, (*2*) solenoid section, (*3*) coaxial current guides to the sections, and (*4*) output flange of the magnetic shield.

TABLE 1. Parameters of the sections of the solenoid and the shield.

| | |
|---|---|
| shield material | Steel 10 |
| External radius and the length and thickness of the shield pipe, mm | 135; 2046; 12 |
| Aperture of the side flanges of the shield, mm | 246 |
| External radius and the length and thickness of the copper solenoid winding, mm | 92; 1000; 5.2 |
| Maximum current in the section windings ($t = 10$ ms), kA | 1.45 |
| Component $B_z$ on the axis at the center of the magnetic system ($t = 11.4$ ms), T | 0.56 |

the specific time moments $t$.

Each of the two solenoid sections has a uniform two-layer winding with an internal diameter of 174 mm and the number of turns $N_{\text{turns}} = 319$. The coils are made of a copper conductor wire with a rectangular $2 \times 6$ mm cross section. Under these conditions, the total length of the solenoid is 2046 mm. The minor decrease in the field within the interval of the solenoid, where the intersectional gap with a length of 4 mm is localized, is compensated by winding the third layer of two additional turns on the intervals of the sections, which are adjacent to this gap.

The choice of the way to ensure the required configuration of the magnetic field in the vacuum chamber of the FEL was based on the numerical simulation performed in the Opera software suite, which allows one to use the finite element method in order to solve the problem of finding the quasistationary magnetic fields allowing for the skin effect in the system of current conductors, as well as tailor-made conducting and magnetic bodies. The model takes into account the pulsed character of the current in the windings of the solenoid and undulator and the magnetic properties of the shield material (steel 10) allowing for the nonlinear magnetization curve, as well as the skin effect in the conducting materials (stainless steel of grade X18H10T and copper M0) used to manufacture the elements of the FEL generator. The following values of material conduction were used in the simulation: $6.9 \times 10^6$ S/m for steel 10, $1.37 \cdot 10^6$ S/m for stainless steel X18H10T, and $5.7 \cdot 10^7$ S/m for copper M0. To reduce the influence of azimuthal conduction currents in the walls of the shield pipe on the magnetic field at the system axis, longitudinal slits that break these currents are included in the design of the shield. These slits 200 mm long and 2 mm wide are made in eight rows with a period of 217 mm in the direction aligned with the shield axis. The angle between the neighboring row is 45°, and the order of the slits in the adjacent rows is shifted by a half-period. On the one hand, this position of the slits makes the design of the shield and the solenoid fixed in it sufficiently rigid, and, on the other hand, allows one to avoid the 10% decrease in the field on the solenoid axis by the azimuthal current in the shield.

Figure 3*a* shows the calculated distribution of the magnetic field on the shield surface at the maximum current in the solenoid. The dependences of the current $I$ in a winding of the solenoid and the stored energy of the magnetic field $E = \int \left( \int \mathbf{B}\, \mathrm{d}\mathbf{H} \right) \mathrm{d}V$ and $E' = \int \left( \int \mathbf{H}\, \mathrm{d}\mathbf{B} \right) \mathrm{d}V$ (here, $\mathbf{B}$ and $\mathbf{H}$ are the induction and strength of the magnetic field, respectively) of the system on the time $t$, as well as the components $B_z$ of the magnetic field on the axis at the center of the solenoid are shown in Figs. 3*b*, 3*c*, and 3*d*, respectively. It is evident from Fig. 3*d* that the maximum value of the magnetic-field induction has the required value 0.56 T at the time moment 11.4 ms, which is quite satisfactory from the viewpoint of the requirements imposed on the magnetic system.

Figure 4 shows the simulated distributions of the component $B_z$ of the magnetic field of the solenoid along the system axis at different time moments. It is evident that the decision made about the distribution of the turns in the windings of the solenoid sections ensures maintenance of good homogeneity of the field at the solenoid axis. The presence of additional turns in the vicinity of the gap between the windings of the two sections counterbalances the decrease in the field induction at this interval with an accuracy of 2%, which is quite sufficient to reduce the amplitude of the spurious cyclotron oscillations of the beam electrons arising due to the inhomogeneity of the solenoid magnetic field.

To check operability of the developed sections of the solenoid and their resistance to electric breakdowns and mechanical damages, we made a prototype of this device and performed test experiments on

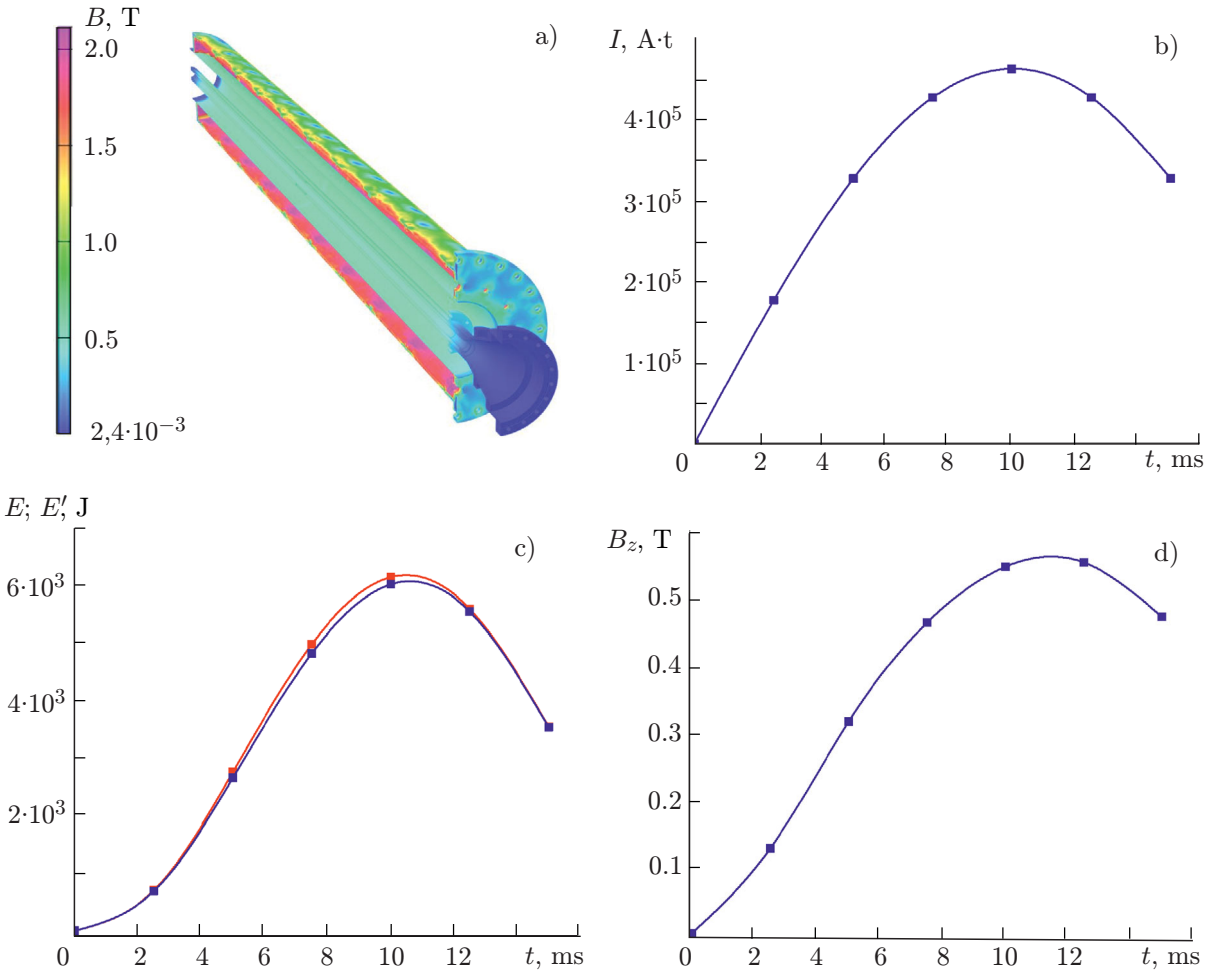


Fig. 3. Distribution of the magnetic field over the shield surface at the maximum current in the solenoid (*a*), time dependence of the current in the solenoid section in ampere–turns (*b*), time dependence of the stored energy of the magnetic field in the solenoid sections (*c*, the red and blue lines correspond to $E$ and $E'$, respectively), and time dependence of the component $B_z$ of the magnetic field on the axis of the solenoid at its center (*d*).

generation of the required magnetic field in it. A photo of the section prototype is shown in Fig. 5*a*, and the electrical diagram of the setup used to test the section, in Fig. 5*b*. As can be seen in the diagram, a bank of capacitors with a total capacitance of 9 mF can be charged up to 5 kV and then switched by means of a thyristor switch to the prototype of the solenoid section. This version of the prototype had a winding with a resistance of 0.2 Ω and an inductance of 2.25 mH. The current through the tested sample in the discharge circuit was measured using a HAZ 10000-SB pulse current sensor. The experiments performed at the charging voltage of the accumulator equal to 1 kV allowed us to achieve a current pulse with an amplitude of 1.4 kA and a duration of 14 ms (see Fig. 6), which corresponded to a magnetic field of 0.6 T at the center of the section.

It should be emphasized that the results of the set of the experiments in the specified regime of operation of the section prototype confirmed the resistance of the prototype to mechanical damages in a great number of current propagation pulses. This demonstrates the adequacy of the developed design of the section for the task of achieving the required induction in the LIA solenoid. At the same time, it was found in the experiments with an increased voltage pulse amplitude that the interlayer insulation is insufficient for the increase in amplitude above 1.1 kV. Based on this result, we decided to enhance the interlayer insulation when manufacturing sections for the working variant of the solenoid.

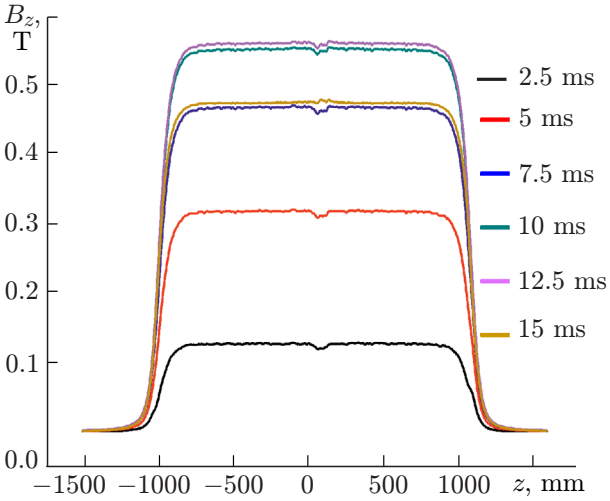


Fig. 4. Time dependence of the $B_z$ component of the magnetic field at the axis of the FEL section system.

To check whether the parameters of the magnetic field in the developed solenoid are adequate for the requirements imposed on the transportation of the beam in the FEL, we modeled the passage of the beam with a current of 1 kA at an electron energy of 5–7 MeV. It was found that such a solenoid could indeed ensure smooth compression of the cross section of the electron beam from the initial state 40 mm in diameter to the final diameter (6 mm) with the amplitude of oscillations of the beam envelope in the region of the homogeneous magnetic field, which did not exceed 1 mm. It was also noted in the modeling process that the oscillations of the beam envelope, which could arise in the process of compression of the cross section of the beam, when the beam enters the magnetic field of the solenoid, could result in the loss of electrons at the walls of the electrodynamic system. Moreover, it turned out that there exists another mechanism of beam electron losses, which is related to bending of the axial magnetic field line of the solenoid. This bending can lead to precipitation of a noticeable fraction of the beam on the wall of the electrodynamic system even at a low angle of deviation of the field line from the direction of the vacuum chamber axis at a significant length (about 2 m) within the solenoid. To prevent such losses, the position of the axial line of the magnetic field will be measured on a special setup and adjusted appropriately already at the stage of solenoid testing before it is installed in a FEL for experiments with the electron beam. The planned installation of additional two-coordinate dipole correction coils, which are fed with a preset d.c. current, will ensure tuning of the directions of the field lines relative to the axis of the vacuum chamber.

### 3.2. Helical undulator

The second important element of the FEL magnetic system is an active helical undulator designed for pumping of the transverse beam oscillations. It should be noted that when choosing the design of the undulator for the use in the magnetic system of the developed FEL generator with an LIA electron beam, we draw on the experience of the earlier successful experiments on creating a free-electron maser, which were performed on the LIU-3000 induction accelerator generating electron beams with a particle energy of 0.8 MeV, a current of 200 A, and a pulse duration of 250 ns at the Joint Nuclear Research Institute (JNRI, Dubna) in cooperation with IAP RAS [43].

In order to improve the distribution homogeneity of the transverse magnetic field of the undulator over the cross section of the beam drift pipe and increase the ratio of the magnetic field of the undulator and

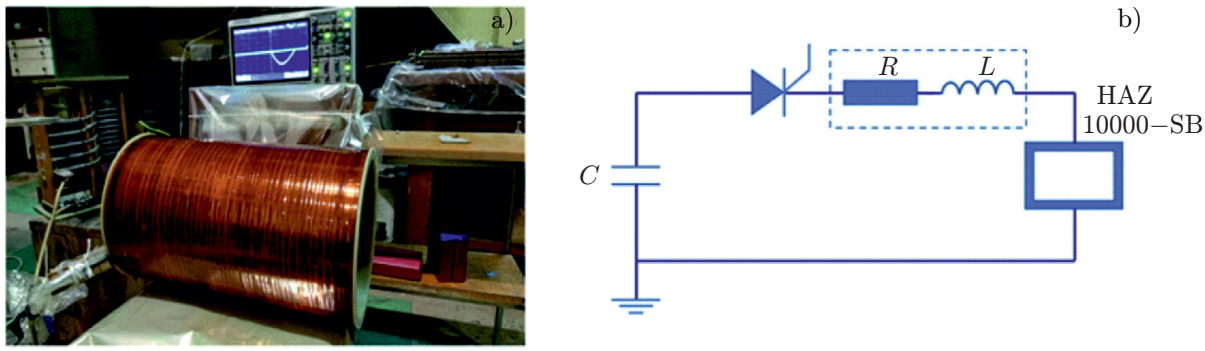


Fig. 5. Photo of the prototype of a shortened solenoid section (*a*) and the electric scheme of the test setup for measurements of the current in the windings of the solenoid (marked with a frame of a dashed line).

the current in the windings, we propose using the bifilar scheme with four helical conductors (see Fig. 7), where the conductors with identical current directions are located at an azimuth angle of 60° to each other and inversely with regard to the conductors with the reverse current direction [44, 45]. Such a position of the current conductors of the undulator in combination with the external homogeneous magnetic field directed along the system axis forms a magnetic configuration with the helical field lines near the axis.

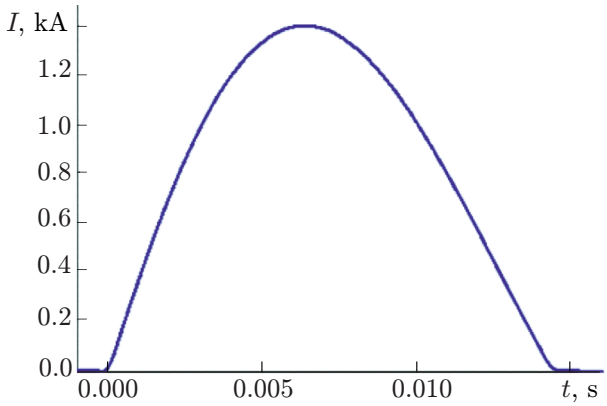


Fig. 6. Time dependence of the current through the windings in the prototype of the shortened section of the magnetic-system solenoid.

Two regimes of FEL operation with the beam are known to exist in a helical magnetic field formed by a uniform longitudinal magnetic field and the transverse undulator magnetic field with the amplitude which increases smoothly along the length $L_{\text{in}}$ [46, 47]. The first regime is characterized by the coincidence of the direction of rotation of the beam electrons in the longitudinal magnetic field with the direction of their rotation in the helical undulator field when the electron move along the direction of the beam propagation. A distinctive feature of this FEL operation regime is the fast decrease in the efficiency of the beam interaction with the generated wave with an increase in the initial angular spread of the beam electrons, as well as with the increase in the deviation from the adiabatic motion of electrons in the transitional region with the length $L_{\text{in}}$, where the amplitude of the undulator field grows from zero to a constant value. The following condition should be fulfilled to maintain adiabaticity of this motion:

$$L_{\text{in}} \gg 2\pi V_{||}/||\Omega_{\text{b}}| - |\omega_H||, \tag{1}$$

where $\Omega_{\text{b}} = 2\pi V_{||}/d_{\text{u}}$ is the bounce frequency, $d_{\text{u}}$ is the undulator period, $\omega_H = eB_0/(\gamma mc)$ is the relativistic gyrofrequency of the electrons in the undulator, $B_0$ is the induction of the guiding field, $V_{||}$ is the longitudinal particle velocity, $e$ and $m$ are the electron charge and mass, respectively, $\gamma$ is the Lorentz factor, and $c$ is the speed of light in vacuum.

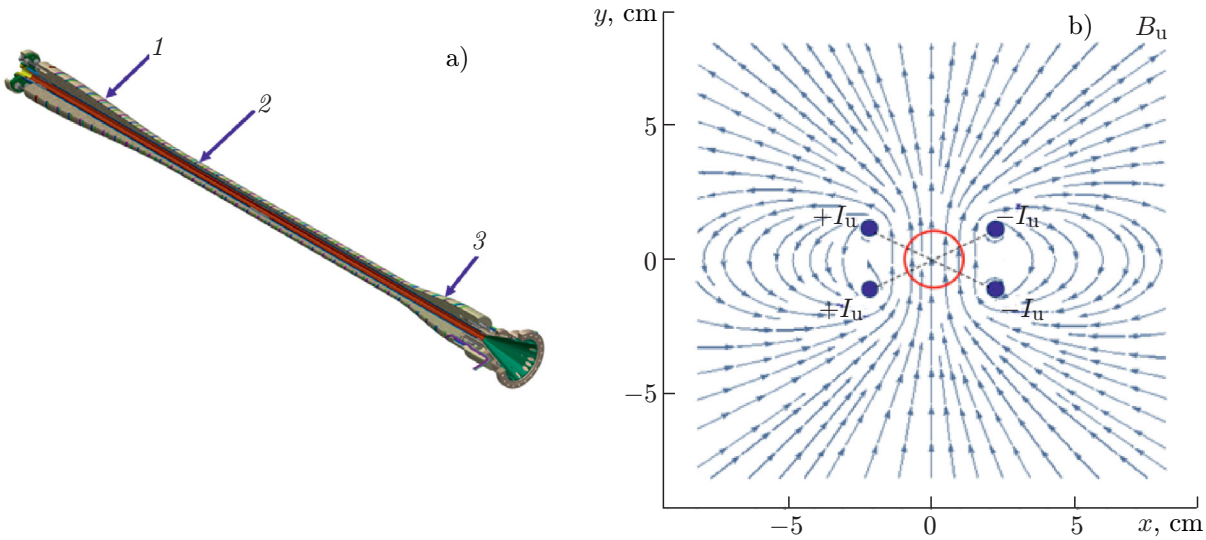


Fig. 7. Three-dimensional model of the helical undulator with the period $d_u = 10$ cm (*a*) and its input (*1*), regular (*2*), and output (*3*) sections. Undulator conductors are shown in different colors. (*b*) Layout of conductor connections in the helical windings of the undulator and the lines of the magnetic field $B_{\text{u}}$ in the transverse section of the regular section.

TABLE 2. Parameters of the undulator.

| | |
|---|---|
| Lengths of the input ($L_{\text{in}}$) and output ($L_{\text{out}}$) parts of the undulator, cm | 65.8, 28.9 |
| Diameter and length of regular part, mm | 48, 1000 |
| Maximum current in the undulator windings ($t = 10$ ms), kA | 15 |
| Amplitudes of the $B_x$ and $B_y$ components at the axis in the central part ($t = 11.4$ ms), T | 0.21, 0.21 |

In contrast to the first regime, in the second magnetic-field operation regime, the electrons rotate in the longitudinal homogeneous field and in the helical field of the undulator in the opposite directions. Under these conditions, the spatial beat period of the bounce oscillations and the cyclotron rotation decreases noticeably and, therefore, the length of the transitional region should satisfy a milder condition, which is significantly easier to fulfill in an experiment:

$$L_{\text{in}} \gg 2\pi V_{||}/(|\Omega_{\text{b}}| + |\omega_H|). \tag{2}$$

Moreover, it was shown in [47] that this regime of the beam interaction with the wave is characterized by a weak dependence of the efficiency of radiation generation on the initial angular spread of the electron velocities. Due to these advantages, we chose the second magnetic-field regime in preference to the other for the experiments on generation of terahertz radiation. For typical values of the longitudinal magnetic field (0.5 T) and an undulator field period of 10 cm, the chosen length of the transitional region (66 cm) satisfies conservatively condition (2) where the ratio of left- and right-hand sides is about 10 for the specified value.

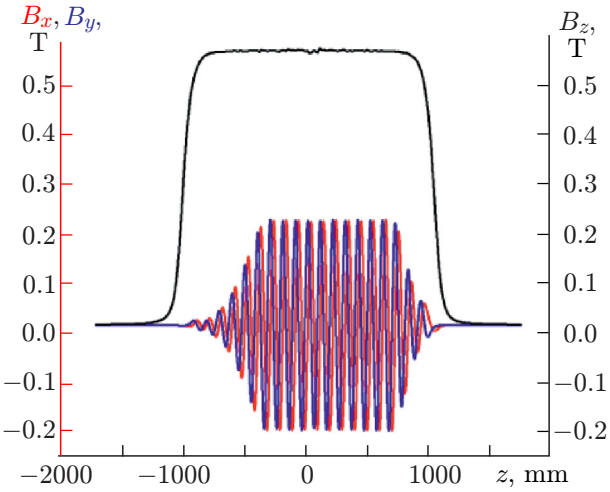


Fig. 8. Distribution of the components $B_x$ and $B_y$ of the undulator magnetic field on the axis of the undulator with the spatial period $d_{\text{u}} = 10$ cm (the $B_z$ component of this field at the axis is almost zero). The component of the field generated by the solenoid of the magnetic system at the axis is shown as $B_z$ in the figure.

To achieve the required smoothness of the increase and decrease in the magnetic field of the undulator, we use the specially chosen configuration of the spiral winding. As shown in Fig. 7*a*, this winding consists of three parts, namely, the input part *1*, the uniform part *2*, and the output part *3*. The main parameters of these three parts are shown in Table 2. The configuration of the conductors in the cross-section of the longest, uniform part of the undulator winding is shown in Fig. 7*b*. The helical conductors with the identical current directions are located at an angle of 60° at a radius of 24 mm, and those with opposite signs are mirror-symmetric in this cross section and further within the uniform winding. As the winding passes over to the input part of the undulator, the conductors with the opposing currents transform gradually to a radius of 43 mm, and the difference in their positions along the azimuthal coordinate decreases monotonically till they become zero. In the output part of the undulator, the conductors also transform from a radius of 24 mm to a radius of 43 mm, while the conductors with the opposing currents diverge in the azimuth angle by 180°. The main geometric and physical parameters of the undulator are listed in Table 2.

The Opera software suite was used to perform three-dimensional simulation of the spatial distribution of the magnetic field generated by the currents in the windings of the developed undulator and two sections of the solenoid. The distributions of the longitudinal magnetic field and its transverse components on the system axis, which were obtained with allowance for the skin effect in various conducting details and elements of the FEL section, are shown in Fig. 8. It is seen in the figure that the above-described configuration of helical windings ensures a smooth increase, the required homogeneity in the main working (regular) section of the undulator, and a smooth decrease in the amplitude of the undulator magnetic field.

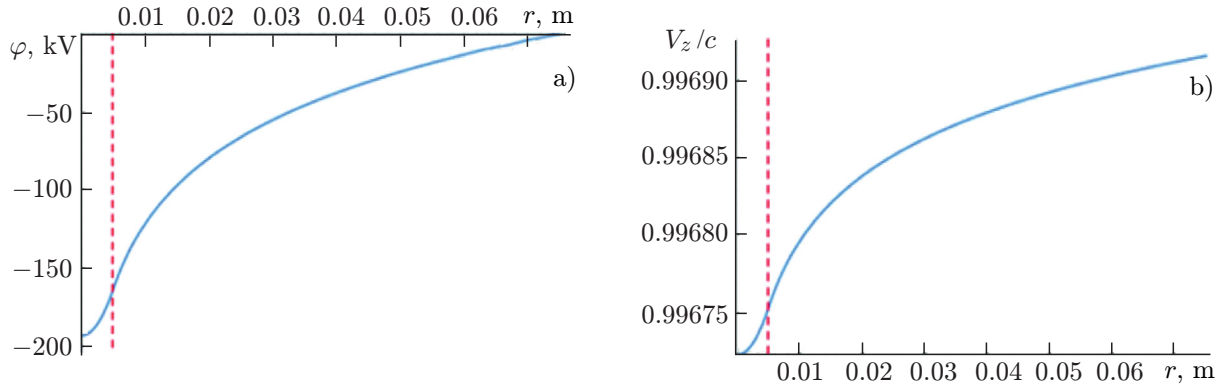


Fig. 9. Distributions of the potential (*a*) and the beam particle velocity (*b*) as functions of the distance counted from the axis of the vacuum channel of the beam drift to the channel boundary (the pipe radius is $r_t = 0.075$ m). The red color shows the boundary of the beam corresponding to the radius $r_\mathrm{b} = 5$ mm.

### 3.3. Calculation of the dynamics of the electron beam in the FEL

The beam dynamics was simulated using the three-dimensional CST Studio Suite code with allowance for the own electric and magnetic fields of the beam during its motion in the combination of the undulator and guiding magnetic fields generated by the FEL magnetic system. It should be noted that in order to solve the problem about beam transportation in the magnetic system of the FEL, we used such boundary conditions, which would not perturb the starting trajectories and emittance of the beam. To do this, we used the conditions of the soft start of particles, which were described at large in [48]. One can mention briefly that in this formulation of the problem the electron beam particles were emitted perpendicularly to the end of the simulation region. The current tube method was chosen as the calculation method, and the total number of current tubes used was 10609. This number of current tubes was determined by the fact that the starting positions of the beam electrons were specified according to the distribution of the Fresnel zones. This is necessary to ensure the uniform density of the charge of the current tubes over the cross section of the beam. Figure 9 shows the specified distributions of the potential in the vacuum drift tube under the conditions of the soft start and the longitudinal velocity of the beam electrons, which were found by solving the problem about the equilibrium distribution of the potential in the tube with allowance for the space charge of the electrons in a cylindrical beam [48]. In this case, the boundary conditions were imposed on the normal components of the electric and magnetic fields in the starting plane: $E_n = 0$ and $B_n = 0$. The grid size chosen for splitting of the computation domain in the transverse cross section was 0.5 mm, which corresponds to 20 computation nodes for the size of the cross section of the electron beam. The longitudinal grid size was 1 mm.

Figure 10 shows an example of the results obtained by simulating transportation of the beam with a particle energy of 6 MeV and a current of 1 kA in a smooth drift tube with the diameter equal to the diameter of the FEL cavity in the magnetic field of two sections of the solenoid and the undulator having the above-described design with the spatial period $d_\mathrm{u} = 10$ cm. In this case, the imported magnetic fields of the compression solenoid and the helical undulator had a characteristic grid size of 1 mm in the longitudinal and transverse directions. The total number of computation nodes for the imported fields was about a million and a half, which is known sufficient to calculate the dynamics of the beam electron trajectories with good accuracy.

It should be noted that we chose the regime of the reverse guiding field as the operating regime of the FEL generator operation [49, 50]. According to the results of the performed simulation, this regime is characterized by low sensitivity to the initial angular spread of the beam electron velocities, as well as high quality of formation of induced transverse electron oscillations by the magnetic field of the undulator. The simulation also showed that in this operation regime the characteristic ratios of the amplitude of spurious cyclotron oscillations to the amplitude of the operating bounce oscillations acquired by the electrons in the

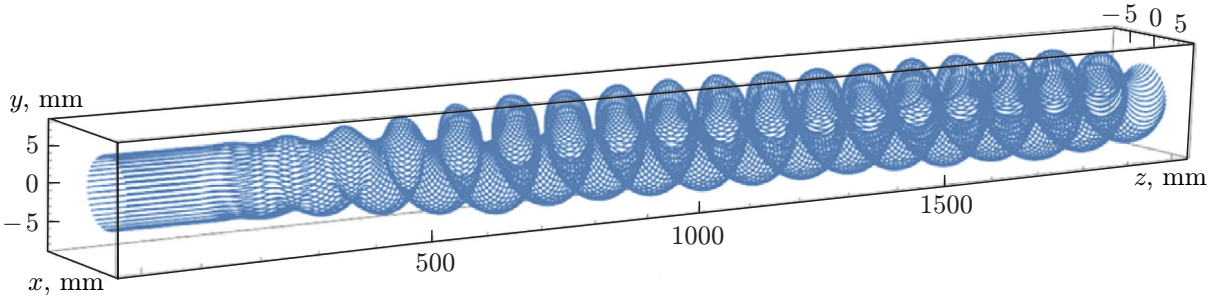


Fig. 10. Electron trajectories obtained by simulating the motion of a high-current relativistic electron beam in the magnetic field produced by sections of the solenoid and the undulator. The figure shows the trajectories of the electrons starting from the boundary of the FEL selection on entering the undulator (the beam particle energy is 6 MeV, the beam current is 1 kA, $d_{\mathrm{u}} = 10$ cm, the beam diameter is 10 mm, the undulator field is 0.15 T, and the magnetic field of the compression solenoid, which is reverse to the propagation direction of the electron beam transported in the FEL section, is 0.8 T).

undulator did not exceed 2–3% in the entire calculation range of variations of the magnetic fields generated by the solenoid and the undulator ($B_0$ and $B_{\mathrm{u}}$, respectively). Thus, the simulation demonstrated the possibility of stable transportation of a high-current electron beam in the calculated magnetic fields of the FEL with the buildup of the amplitude of transverse undulator oscillations to the required value, which indicates that it is possible to achieve efficient electron-wave interaction in the subterahertz/terahertz FEL generator with a relatively high electron efficiency.

## 4. CONCLUSIONS

We have arrived at an engineering solution for realization of the FEL generator project in the 0.3–1.2 THz frequency range based on a kiloampere electron beam formed in LIA with a particle energy of 5–10 MeV. Within the framework of this solution, we designed the main project systems and elements including a vacuum chamber for beam transportation and a magnetic system for generation of the required configuration of the magnetic field which ensures both the buildup of working oscillations of the beam electrons, and the compression of the beam cross section and stable transportation of the beam in the FEL cavity. The results of the simulation and bench tests demonstrated that the developed main units of the FEL satisfy the conditions of the experiments on generation of terahertz waves in a FEL generator. Tests of the manufactured prototype of a solenoid section showed that it was operable in the range of operating voltages up to 1 kV, and it was possible to achieve a field strength of more than 0.5 T after improvement of the interlayer insulation.

Based on the results of simulating the dynamics of the electron beam in the process of its transportation in the drift tube under the conditions of the superposition of the magnetic fields generated by the solenoid and the undulator, it was shown that the reverse-field regime has low sensitivity to the initial spread in the parameters of the electron beam.

At present, the helical undulator is being manufactured according to the developed design.

The obtained results form the reliable basis for realization of the project of a terahertz FEL generator, which would allow generating pulses of coherent subgigawatt radiation in accordance with the scheme of interaction of long-pulse LIA beams with highly selective electrodynamic systems for a pulse duration of about 100 ns.

This work was partially supported by the Russian Science Foundation (Project No. 19–12–00212).

**REFERENCES**


1. A. V. Arzhannikov, N. S. Ginzburg, A. M. Malkin, et al., *Proc. 44th Int. Conf. Infrared, Millimeter, and Terahertz Waves (IRMMW-THz 2019). 1–6 September 2019, Paris, France*, Art. no. 5864231. https://doi.org/10.1109/IRMMW-THz.2019.8874573
2. N. Yu. Peskov, A. V. Arzhannikov, N. S. Ginzburg, et al., *Proc. SPIE. V. 11582. 4th Int. Conf. Terahertz and Microwave Radiation: Generation, Detection, and Applications. 24–26 August 2020, Tomsk, Russia*, 1158207. https://doi.org/10.1117/12.2579554
3. P. V. Logachev, G. I. Kuznetsov, A. A. Korepanov, et al., *Instrum. Exp. Tech.*, No. 6, 42–49 (2013). https://doi.org/10.7868/S0032816213060220
4. D. A. Nikiforov, M. F. Blinov, V. V. Fedorov, et al., *Phys. Part. Nuclei Lett.*, **17**, 197–203 (2020). https://doi.org/10.1134/S1547477120020156
5. E. S. Sandalov, S. L. Sinitsky, D. I. Skovorodin, et al., in: *2021 IEEE Int. Conf. Plasma Science, September 12–16, 2021, Lake Tahoe, USA*, 9588436. https://doi.org/10.1109/ICOPS36761.2021.9588436
6. W. Faries, K. A. Gehring, P. L. Richards, and Y. R. Shen, *Phys. Rev.*, **180**, No. 2, 363–365 (1969). https://doi.org/10.1103/PhysRev.180.363
7. J. R. Morris and Y. R. Shen, *Opt. Commun.*, **3**, No. 2, 81–84 (1971). https://doi.org/10.1016/0030-4018(71)90182-9
8. C. Fattinger and D. Grischkowsky, *Appl. Phys. Lett.*, **53**, 1480–1482 (1988). https://doi.org/10.1063/1.99971
9. D. Grischkowsky, S. Keiding, M. Exter, and Ch. Fattinger, *J. Opt. Soc. Am. B*, **7**, 2006–2015 (1990).
10. P. Shumyatsky and R. R. Alfano, *J. Biomed. Opt.*, **16**, No. 3, 033001 (2011). https://doi.org/10.1117/1.3554742
11. Y. Lee, *Principles of Terahertz Science and Technology (Lecture Notes in Physics)*, Springer, New York (2009).
12. P. Tan, J. Huang, K. Liu, et al., *Sci. China Inf. Sci.*, **55**, 1–15 (2012). https://doi.org/10.1007/s11432-011-4515-1
13. P. U. Jepsen, D. G. Cooke, and M. Koch, *Laser Photonics Rev.*, **5**, 124–66 (2011). https://doi.org/10.1002/lpor.201000011
14. P. C. M. Planken, C. E. Rijmenam, and R. N. Schouten, *Semicond. Sci. Technol.*, **20**, No. 7, S121–S127 (2005). https://doi.org/10.1088/0268-1242/20/7/001
15. K. B. Cooper, R. J. Dengler, N. Llombart, et al., *IEEE Trans. Terahertz Sci. Technol.*, **1**, No. 1, 169–182 (2011). https://doi.org/10.1109/TTHZ.2011.2159556
16. T. Kampfrath, K. Tanaka, and K. A. Nelson, *Nat. Photonics*, **7**, 680–690 (2013). https://doi.org/10.1038/nphoton.2013.184
17. B. L. Yu, Yang Y., Zeng F., et al., *Appl. Phys. Lett.*, **86**, No. 10, 101108 (2005). https://doi.org/10.1063/1.1882759
18. M. Thumm, *J. Infrared Millim. Terahertz Waves*, **41**, 1–140 (2020). https://doi.org/10.1007/s10762-019-00631-y
19. R. A. Lewis, *J. Phys. D, Appl. Phys.*, **47**, 374001 (2014). https://doi.org/10.1088/0022-3727/47/37/374001
20. G. P. Gallerano and S. Biedron, *26th Int. Free Electron Laser Conf. August, 29—September, 3 2004, Trieste, Italy*, p. 216–221.

21. M. Yu. Glyavin, A. G. Luchinin, A. A. Bogdashov, et al. *Radiophys. Quantum Electron.*, **56**, Nos. 8–9, 497–507 (2014). https://doi.org/10.1007/s11141-014-9454-4

22. A. V. Arzhannikov and I. V. Timofeev, *Plasma Phys. Control. Fusion* **54**, 105004 (2012). https://doi.org/10.1088/0741- 3335/54/10/105004

23. A. V. Arzhannikov, I. A. Ivanov, A. A. Kasatov, et al., *Plasma Phys. Control. Fusion*, **62**, No. 4, 045002 (2020). https://doi.org/10.1088/1361-6587/ab72e3

24. I. V. Timofeev, V. V. Annenkov, and A. V. Arzhannikov, *Phys. Plasmas*, **22**, 113109 (2015). https://doi.org/10.1063/1.4935890

25. D. A. Samtsov, A. V. Arzhannikov, S. L. Sinitsky, et al., *IEEE Trans. Plasma Sci.*, **49**, No. 11, 3371–3376 (2021). https://doi.org/10.1109/TPS.2021.3108880

26. A. V. Arzhannikov, S. L. Sinitsky, S. S. Popov, et al., *IEEE Trans. Plasma Sci.*, **50**, No. 8, 2348–2363 (2022). https://doi.org/10.1109/TPS.2022.3183629

27. A. Arzhannikov, V. Annenkov, I. Ivanov, et al., *J. Phys. Conf. Series*, **1647**, No. 1, 012010 (2020). https://doi.org/10.1088/1742-6596/1647/1/012010

28. G. P. Gallerano, A. Doria, E. Giovenale, et al., *Terahertz Sci. Technol.*, **7**, No. 4, 160–171 (2014). https://doi.org/10.11906/TST.160-171.2014.12.15

29. Y. U. Jeong, B. C. Lee, S. K. Kim, et al., *Nucl. Instrum. Methods Phys. Res. A*, **475**, Nos. 1–3, 47–50 (2001). https://doi.org/10.1016/S0168-9002(01)01533-9

30. J. Byrd, M. W. P. Leemans, A. Loftsdottir, et al., *Phys. Rev. Lett.*, **89**, 224801 (2002). https://doi.org/10.1103/PhysRevLett.89.224801

31. G. L. Carr, M. C. Martin, W. R. McKinney, et al., *Nature*, **420**, 153–156 (2002). https://doi.org/10.1038/nature01175

32. A. Gover, A. Faingersh, A. Eliran, et al., *Nucl. Instrum. Methods Phys. Res. A*, **528**, 23–27 (2004). https://doi.org/10.1016/j.nima.2004.04.011

33. A. F. G. Van der Meer, *Nucl. Instrum. Methods Phys. Res. A*, **528**, 8–14 (2004). https://doi.org/10.1016/j.nima.2004.04.008

34. O. A. Shevchenko, V. S. Arbuzov, N. A. Vinokurov, et al., *Phys. Procedia*, **84**, 13–18 (2016). https://doi.org/10.1016/j.phpro.2016.11.004

35. G. N. Kulipanov, E. G. Bagryanskaya, E. N. Chesnokov, et al., *IEEE Trans. Terahertz Sci. Technol.*, **5**, No. 5, 798–809 (2015). https://doi.org/10.1109/TTHZ.2015.2453121

36. D. A. Nikiforov, A. V. Petrenko, S. L. Sinitsky, et al., *J. Instrum.*, **16**, P11024 (2021). https://doi.org/10.1088/1748-0221/16/11/P11024

37. D. A. Nikiforov, A. V. Ivanov, S. L. Sinitsky, et al., *Siberian J. Phys.*, **17**, No. 4, 31–44 (2022). https://doi.org/10.25205/2541-9447-2022-17-4-31-44

38. E. S. Sandalov, S. L. Sinitsky, D. A. Nikiforov, et al., *Proc. 46th Int. Conf. Infrared, Millimeter and Terahertz Waves. August 29—September 3, 2021, Chengdu, China*, 9567073. https://doi.org/10.1109/IRMMW-THz50926.2021.9567073

39. E. S. Sandalov, S. L. Sinitsky, D. I. Skovorodin, et al., *Siberian J. Phys.*, **17**, No. 2, 16–29 (2022). https://doi.org/10.25205/2541-9447-2022-17-2-16-29

40. E. S. Sandalov, S. L. Sinitsky, A. V. Arzhannikov, et al., *Bull. Rus. Acad. Sci. Phys.*, **87**, No. 5, 573–579 (2023). https://doi.org/10.3103/S1062873822701763

41. A. V. Arzhannikov, P. A. Bak, V. I. Belousov, et al., *Radiophys. Quantum Electron.*, **64**, No. 11, 814–824 (2022). https://doi.org/10.1007/s11141-022-10180-5

42. N. Yu. Peskov, A. V. Arzhannikov, V. I. Belousov, et al, *Proc. XI All-Russia Scientific-Technical Conf. "Microwave Electronics and Microelectronics," May 30—June 2, 2022, St. Petersburg, Russia*, pp. 207–211.

43. A. K. Kaminsky, É. A. Perel'stein, S. N. Sedykh, et al., *Tech. Phys. Lett.*, **36**, No. 3, 211–215 (2010). https://doi.org/10.1134/S1063785010030053

44. N. Yu. Peskov, N. S. Ginzburg, A. K. Kaminsky, et al., *Proc. 41th Int. Conf. Infrared, Millimeter and Terahertz Waves. September 25–30, 2016, Copenhagen, Denmark*, 7758360. https://doi.org/10.1109/IRMMW-THz.2016.7758360

45. N. Yu. Peskov, N. S. Ginzburg, A. K. Kaminsky, et al., *Radiophys. Quantum Electron.*, **63**, No. 12, 931–975 (2021). https://doi.org/10.1007/s11141-021-10105-8

46. N. S. Ginzburg and N. Yu. Peskov, *Zh. Tekh. Fiz*, **58**, No. 5, 859–869 (1988).

47. N. Yu. Peskov, *High-Power Free-Electron Masers with One- and Two-Dimensional Distributed Feedback*, Doct. Sci. Theses, Nizhny Novgorod (2011).

48. E. S. Sandalov, S. L. Sinitsky, D. I. Skovorodin, et al., *IEEE Trans. Plasma Sci.*, **49**, No. 9, 2737–2749 (2021). https://doi.org/10.1109/TPS.2021.3105661

49. A. A. Kaminsky, A. K. Kaminsky, S. B. Rubin, et al., *Part. Accel.*, **33**, 189–194 (1990).

50. M. E. Conde and G. Bekefi, *Phys. Rev. Lett.*, **67**, No. 22, 3082–3085 (1991). https://doi.org/10.1103/PhysRevLett.67.3082